Inorganic Chemistry
Article

Inorg. Chem. **2010**, *49*, 3239–3251 **3239**
DOI: 10.1021/ic902094c

Structural and Luminescence Studies on $\pi\cdots\pi$ and Pt$\cdots$Pt Interactions in Mixed Chloro-Isocyanide Cyclometalated Platinum(II) Complexes†

Álvaro Díez,[‡] Juan Forniés,[§] Carmen Larraz,[§] Elena Lalinde,*[,‡] José A. López,[§] Antonio Martín,[§] M. Teresa Moreno,*[,‡] and Violeta Sicilia[∥]

[‡]*Departamento de Química - Grupo de Síntesis Química de La Rioja, UA-CSIC, Universidad de La Rioja, 26006, Logroño, Spain,* [§]*Departamento de Química Inorgánica, Instituto de Ciencia de Materiales de Aragón, Facultad de Ciencias, Universidad de Zaragoza-CSIC, Plaza S. Francisco s/n 50009 Zaragoza, Spain, and* [∥]*Departamento de Química Inorgánica, Instituto de Ciencia de Materiales de Aragón, Escuela Universitaria de Ingeniería Técnica Industrial, Universidad de Zaragoza-CSIC, Campus Universitario del Actur, Edificio Torres Quevedo, 50018, Zaragoza, Spain*

Received October 22, 2009

[Pt(bzq)Cl(CNR)] [bzq = benzoquinolinate; R = *tert*-butyl (^{t}Bu **1**), 2-6-dimethylphenyl (Xyl **2**), 2-naphthyl (2-Np **3**)] complexes have been synthesized and structurally and photophysically characterized. **1** was found to co-crystallize in two distinct pseudopolymorphs: a red form, which exhibits an infinite 1D-chain ($[\mathbf{1}]_\infty$) and a yellow form, which contains discrete dimers ($[\mathbf{1}]_\mathbf{2}$), both stabilized by interplanar $\pi\cdots\pi$ (bzq) and short Pt$\cdots$Pt bonding interactions. Complex **3**, generated through the unexpected garnet-red double salt isomer $[Pt(bzq)(CN\text{-}2\text{-}Np)_2][Pt(bzq)Cl_2]$ **4**, crystallizes as yellow Pt$\cdots$Pt dimers ($[\mathbf{3}]_\mathbf{2}$), while **2** only forms $\pi\cdots\pi$ (bzq) contacting dimers. Their electronic absorption and luminescence behaviors have been investigated. According to Time-Dependent Density Functional Theory (TD-DFT) calculations, the lowest-lying absorption (CH_2Cl_2) has been attributed to combined ^{1}ILCT and ^{1}MLCT/^{1}ML′CT (L = bzq, L′ = CNR) transitions, the latter increasing from **1** to **3**. In solid state, while the yellow form $[\mathbf{1}]_\mathbf{2}$ exhibits a green ^{3}MLCT unstructured emission only at 77 K, the 1-D form $[\mathbf{1}]_\infty$ displays a characteristic low-energy red emission (672 nm, 298 K; 744 nm, 77 K) attributed to a mixed ^{3}MMCT [d(σ^*)→p(σ)]/^{3}MMLCT [dσ^*(M_2)→$\sigma(\pi^*)$(bzq)] excited state. However, upon exposure to standard atmospheric conditions, $[\mathbf{1}]_\infty$ shows an irreversible change to an orange-ochre solid, whose emissive properties are similar to those of the crude **1**. Complexes **2** and **3** (77 K) exhibit a structured emission from discrete fragments (^{3}LC/^{3}MLCT), whereas the luminescence of the garnet-red salt **4** is dominated by a low energy emission (680 nm, 298 K; 730 nm, 77 K) arising from a ^{3}MMLCT excited state. Solvent (CH_2Cl_2, toluene, 2-MeTHF and CH_3CN) and concentration-dependent emission studies at 298 K and at 77 K are also reported for **1**−**3**. In CH_2Cl_2 solution, the low phosphorescent emission band is ascribed to bzq intraligand charge transfer ^{3}ILCT mixed with metal-to-ligand (L = bzq, L′ = CNR) charge transfer ^{3}MLCT/^{3}ML′CT character with the Pt to CNR contribution increasing from **1** to **3**, according to computational studies.

Introduction

Luminescent cyclometalated platinum(II) complexes is a topic of current research and has recently been the subject of excellent comprehensive reviews.[1−7] Many of such complexes prove to be luminescent even in solution under ambient conditions, and this is a feature that has led to the recent interest in them as triplet emitters in organic light emitting devices (OLEDs)[2,3,8−18] or as interesting biosignaling

† Dedicated to Prof. N. G. Connelly on the occasion of his retirement.

*To whom correspondence should be addressed. E-mail: elena.lalinde@unirioja.es (E.L.); teresa.moreno@unirioja.es (M.T.M.). Fax: (+34)941-299621.

(1) Williams, J. A. G. *Top. Curr. Chem.* **2007**, *281*, 205.
(2) Williams, J. A. G.; Develay, S.; Rochester, D. L.; Murphy, L. *Coord. Chem. Rev.* **2008**, *252*, 2596.
(3) Williams, J. A. G. *Chem. Soc. Rev.* **2009**, *38*, 1783.
(4) Ma, B.; Djurovich, P. I.; Thompson, M. E. *Coord. Chem. Rev.* **2005**, *249*, 1501.
(5) Yersin, H.; Donges, D. *Top. Curr. Chem.* **2001**, *214*, 81.
(6) Lai, S. W.; Che, C. M. *Top. Curr. Chem.* **2004**, *241*, 27.
(7) Kato, M. *Bull. Chem. Soc. Jpn.* **2007**, *80*, 287.
(8) Evans, R. C.; Douglas, P.; Winscom, C. J. *Coord. Chem. Rev.* **2006**, *250*, 2093.
(9) Williams, J. A. G. Molecular Organometallic Materials for Optics. In *Topics in Organometallic Chemistry*; Bozec, H., Guerchais, V., Eds.; Springer: New York, 2009; Vol. *28*.
(10) Xiang, H. F.; Lai, S. W.; Lai, P. T.; Che, C. M. Phosphorescent platinum(II) materials for OLED applications. In *Highly Efficient OLEDs with Phosphorescent Materials*; Yersin, H., Ed.; Wiley-VCH: Weinheim, Germany, 2007.
(11) Thomas, S. W., III; Venkatesan, K.; Müller, P.; Swager, T. M. *J. Am. Chem. Soc.* **2006**, *128*, 16641.
(12) Laskar, I. R.; Hsu, S. F.; Chen, T. M. *Polyhedron* **2005**, *24*, 881.
(13) Wong, W. Y.; He, Z.; So, S. K.; Tong, K. L.; Lin, Z. *Organometallics* **2005**, *24*, 4079.

© 2010 American Chemical Society
Published on Web 03/10/2010

species.[19] In these complexes, emission typically originates from ligand centered (^{3}LC) and/or metal-to-ligand charge transfer (^{3}MLCT) states. In addition, some square-planar Pt(II) complexes with sterically undemanding ligands have tendency to form stacking structures or dimers controlled by Pt···Pt and/or $\pi\cdots\pi$ interactions, that exhibit red-shifted phosphorescence derived from metal-metal-to-ligand charge transfer (^{3}MMLCT) and/or excimeric excited states.[7,14,20−31] In general, their absorptions and emissions are strongly dependent on the extent of Pt···Pt and/or $\pi\cdots\pi$ interactions, and consequently are highly dependent upon the crystallization solvent, concentration, temperature, or the counterion nature.[23,31−36]

Pt(II)-isocyanide complexes have aroused great interest in recent years as components in luminescent chromophores. In this area, diverse stacked double-salts $[Pt(CNR)_4][M(CN)_4]$ (M = Pt, Pd)[37−46] and mixed [*cis*-$Pt(CN)_2(CNR)_2$][37,47−49] and [*trans*-$Pt(CN\text{-}p\text{-}C_6H_4{-}C_2H_5)_2(CN)_2$][47] compounds, that exhibit vapochromic and vapoluminescent properties, have been reported, and a recent work has revealed that $[Pt(CN\text{-}^tBu)_2(CN)_2]$ forms luminescent 1D nanostructures by Pt···Pt interactions.[50] Despite the fact that related platinum isocyanide chloride systems of formula $[Pt(CNR)_4][PtCl_4]$ and [*cis*-$Pt(CNR)_2Cl_2$] have been long known,[51−54] very few structures have been determined by X-ray crystallography.[55] A recent reinvestigation of [*cis*-$Pt(CNPh)_2Cl_2$] has shown the formation of two different polymorphs under different crystallization conditions. One of them contains vacant channels that are stabilized by a combination of extended Pt···Pt interactions and $\pi\cdots\pi$ stacking.[56]

Pt(II) complexes bearing cyclometalated and isocyanide ligands have revealed interesting photophysical properties,[24,27,28,57] including low-energy emissions in fluid solution. Along these lines, we have recently described the synthesis of the isocyanide benzoquinolate Pt(II) complexes $[Pt(bzq)(CNR)_2]X$ (R = ^{t}Bu, Xyl, 2-Np; X = ClO_4^-, PF_6^-) and the influence of the counteranion and concentration on their luminescent properties.[31] In this report we describe the preparation, structures, and photophysical properties of the neutral complexes [Pt(bzq)Cl(CNR)] (R = ^{t}Bu **1**, Xyl **2**, 2-Np **3**) (Scheme 1). The *tert*-butylisocyanide derivative **1** shows solid-state pseudopolymorphic behavior. X-ray structures are reported for a red form $[\mathbf{1\cdot CHCl_3}]_\infty$ ($[\mathbf{1}]_\infty$), which exhibits an infinite 1-D chain network and for a yellow form $[\mathbf{1\cdot 0.5H_2O}]_\mathbf{2}$ ($[\mathbf{1}]_\mathbf{2}$), which consists of discrete dimers, both based on Pt···Pt and $\pi\cdots\pi$ (bzq) bonding interactions. **2** only forms yellow crystals in which two monomers are weakly contacting through $\pi\cdots\pi$ (bzq) interactions. With the 2-naphthylisocyanide ligand, two isomeric species have been separated, a neutral yellow derivative, which crystallizes as a Pt···Pt dimer, $[Pt(bzq)Cl(CN\text{-}2\text{-}Np)]_2$ ($[\mathbf{3}]_\mathbf{2}$), and the garnet-red double salt $[Pt(bzq)(CN\text{-}2\text{-}Np)_2]^+[Pt(bzq)Cl_2]^-$ **4**. The role of crystal packing and the influence of the CNR ligand on their luminescent properties are reported.

Results and Discussion

Synthesis and Characterization. A bridge splitting reaction in diplatinum halide-bridge complexes is a classic reaction widely used to synthesize mononuclear

(14) Lu, W.; Mi, B. X.; Chan, M. C. W.; Hui, Z.; Che, C. M.; Zhu, N.; Lee, S. T. *J. Am. Chem. Soc.* **2004**, *126*, 4958.
(15) Yang, C.; Zhang, X.; You, H.; Zhu, L.; Chen, L.; Zhu, L.; Tao, Y.; Ma, D.; Shuai, Z.; Qin, J. *Adv. Funct. Mater.* **2007**, *17*, 651.
(16) Ionkin, A. S.; Marshall, W. J.; Wang, Y. *Organometallics* **2005**, *24*, 619.
(17) Yan, B. P.; Cheung, C. C. C.; Kui, S. C. F.; Roy, V. A. L.; Che, C. M.; Xu, S. J. *Appl. Phys. Lett.* **2007**, *91*, 063508.
(18) Qiu, D.; Wu, J.; Xie, Z.; Cheng, Y.; Wang, L. *J. Organomet. Chem.* **2009**, *694*, 737.
(19) Ma, D. L.; Che, C. M.; Yan, S. C. *J. Am. Chem. Soc.* **2009**, *131*, 1835 and references therein.
(20) Anderson, B. M.; Hurst, S. K. *Eur. J. Inorg. Chem.* **2009**, *21*, 3041.
(21) Utsono, M.; Yutaka, T.; Murata, M.; Kurihara, M.; Tamai, N.; Nishihara, H. *Inorg. Chem.* **2007**, *46*, 11291.
(22) Kui, S. C. F.; Chui, S. S. Y.; Che, C. M.; Zhu, N. *J. Am. Chem. Soc.* **2006**, *128*, 8297.
(23) Yam, V. W. W.; Chan, K. H. Y.; Wong, K. M. C.; Zhu, N. *Chem.—Eur. J.* **2005**, *11*, 4535.
(24) Lai, S. W.; Lam, H. W.; Lu, W.; Cheung, K. K.; Che, C. M. *Organometallics* **2002**, *21*, 226.
(25) Poater, A.; Moradell, S.; Pinilla, E.; Poater, J.; Solá, M.; Martínez, M. A.; Llobet, A. *Dalton Trans.* **2006**, 1188.
(26) Ding, J.; Pan, D.; Tung, C. H.; Wu, L. Z. *Inorg. Chem.* **2008**, *47*, 5099.
(27) Lu, W.; Chan, M. C. W.; Cheung, K. K.; Che, C. M. *Organometallics* **2001**, *20*, 2477.
(28) Lai, S. W.; Chan, M. C. W.; Cheung, K. K.; Che, C. M. *Organometallics* **1999**, *18*, 3327.
(29) Lai, S. W.; Chan, M. C. W.; Cheung, K. K.; Peng, S. M.; Che, C. M. *Organometallics* **1999**, *18*, 3991.
(30) Lu, W.; Chan, M. C. W.; Zhu, N.; Che, C. M.; Li, C.; Hui, Z. *J. Am. Chem. Soc.* **2004**, *126*, 7639.
(31) Díez, A.; Forniés, J.; Fuertes, S.; Larraz, C.; Lalinde, E.; López, J. A.; Martín, A.; Moreno, M. T.; Sicilia, V. *Organometallics* **2009**, *28*, 1705.
(32) Tam, A. Y. Y.; Lam, W. H.; Wong, K. M. C.; Zhu, N.; Yam, V. W. W. *Chem.—Eur. J.* **2008**, *14*, 4562.
(33) Tam, A. Y. Y.; Wong, K. M. C.; Wang, G.; Yam, V. W. W. *Chem. Commun.* **2007**, 2028.
(34) Yam, V. W. W.; Wong, K. M. C.; Zhu, N. *J. Am. Chem. Soc.* **2002**, *124*, 6506.
(35) Büchner, R.; Field, J. S.; Haines, R. J.; Cunningham, C. T.; McMillin, D. R. *Inorg. Chem.* **1997**, *36*, 3952.
(36) Büchner, R.; Cunningham, C. T.; Field, J. S.; Haines, R. J.; McMillin, D. R.; Summerton, G. C. *J. Chem. Soc., Dalton Trans.* **1999**, 711.
(37) Buss, C. E.; Mann, K. R. *J. Am. Chem. Soc.* **2002**, *124*, 1031.
(38) Daws, C. A.; Exstrom, C. L.; Sowa, J. R.; Mann, K. R. *Chem. Mater.* **1997**, *9*, 363.
(39) Drew, S. M.; Janzen, D. E.; Buss, C. E.; MacEwan, D. I.; Dublin, K. M.; Mann, K. R. *J. Am. Chem. Soc.* **2001**, *123*, 8414.
(40) Exstrom, C. L.; Pomije, M. K.; Mann, K. R. *Chem. Mater.* **1998**, *10*, 942.
(41) Exstrom, C. L.; Sowa, J. R.; Daws, C. A.; Janzen, D. E.; Mann, K. R.; Moore, G. A.; Stewart, F. F. *Chem. Mater.* **1995**, *7*, 15–17.
(42) Kunugi, Y.; Mann, K. R.; Miller, L. L.; Exstrom, C. L. *J. Am. Chem. Soc.* **1998**, *120*, 589.
(43) Drew, S. M.; Manna, J. E.; Marquardt, B. J.; Mann, K. R. *Sens. Actuators, B* **2004**, *97*, 304.
(44) Buss, C. E.; Anderson, C. E.; Pomije, M. K.; Lutz, C. M.; Britton, D.; Mann, K. R. *J. Am. Chem. Soc.* **1998**, *120*, 7783.
(45) Kunugi, Y.; Miller, L. L.; Mann, K. R.; Pomije, M. K. *Chem. Mater.* **1998**, *10*, 1487.
(46) Grate, J. W.; Moore, L. K.; Janzen, D. E.; Veltkamp, D. J.; Kaganove, S.; Drew, S. M.; Mann, K. R. *Chem. Mater.* **2002**, *14*, 1058.
(47) Dylla, A. G.; Janzen, D. E.; Pomije, M. K.; Mann, K. R. *Organometallics* **2007**, *26*, 6243.
(48) Zhou, X.; Zhang, H. X.; Pan, Q. J.; Li, M. X.; Wang, Y.; Che, C. M. *Eur. J. Inorg. Chem.* **2007**, 2181.
(49) Drew, S. M.; Smith, L. I.; McGee, K. A.; Mann, K. R. *Chem. Mater.* **2009**, *21*, 3117.
(50) Sun, Y.; Ye, K.; Zhang, H. X.; Zhang, J.; Zhao, L.; Li, B.; Yang, G.; Yang, B.; Wang, Y.; Lai, S. W.; Che, C. M. *Angew. Chem., Int. Ed.* **2006**, *45*, 5610.
(51) Hoffmann, K. A.; Bugge, G. *Chem. Ber.* **1907**, *40*, 1772.
(52) Ramberg, L. *Chem. Ber.* **1907**, *40*, 2578.
(53) Bonati, F.; Minghetti, G. *J. Organomet. Chem.* **1970**, *24*, 251.
(54) Keller, H. J.; Lorentz, R. *Anorg. Chem. Org. Chem.* **1976**, *31B*, 565.
(55) Jonavic, B.; Manojlovic-Muir, L.; Muir, K. W. *J. Chem. Soc., Dalton Trans.* **1972**, 1178.
(56) Sluch, I. M.; Miranda, A. J.; Slaughter, L. M. *Cryst. Growth. Des.* **2009**, *9*, 1267.
(57) Lu, W.; Chen, Y.; Roy, V. A. L.; Chui, S. S. Y.; Che, C. M. *Angew. Chem., Int. Ed.* **2009**, *48*, 7621.

Scheme 1

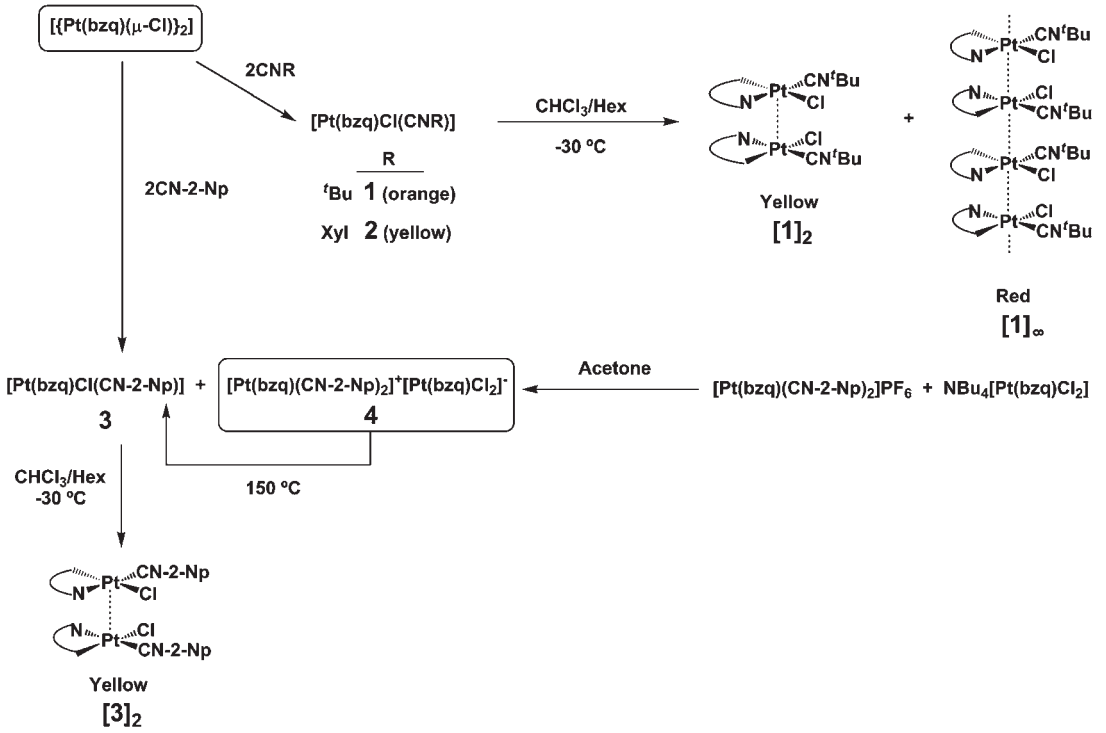

complexes.[58,59] By starting from dinuclear cycloplatinate complexes, final [Pt(C-X)ClL] complexes with the incoming ligand L *cis*- or *trans*- to the metalated carbon are obtained, depending on the electronic and steric requirements of the ligands. Likewise, as is shown in Scheme 1, [Pt(bzq)Cl(CNR)] (R = ^{t}Bu **1**, Xyl **2**) were obtained as orange (**1**) or yellow (**2**) solids in high yield by reaction of [{Pt(bzq)(μ-Cl)}$_2$] with 2 equiv of the corresponding CNR in CH_2Cl_2. Interestingly, while crystallization of [Pt(bzq)-Cl(CN-Xyl)] **2** from different solvents always results in fine yellow needles, which are spectroscopically identical to the initial solid (ν_{CN} at 2181s, 2140sh), slow crystallization ($CHCl_3$/Hexane, −30 °C) of the orange powder **1** (ν_{CN} 2202 cm^{-1}) simultaneously results in yellow [**1**]$_2$ and red [**1**]$_\infty$ crystals (Figure 1), which exhibit slight differences in the ν_{CN} (2185, 2146sh [**1**]$_2$; 2210, 2169sh cm^{-1} [**1**]$_\infty$). The yellow form ([**1**]$_2$) contains 0.5 molecules of H_2O, as has been confirmed by X-ray diffraction studies (see below), and it is stable for months. However, the red crystals ([**1**]$_\infty$) contain one molecule of $CHCl_3$ per monomer, which is rapidly lost, evolving to an orange-ochre powder similar to the initial crude **1** (IR and photophysical properties).

Curiously, when reaction was carried out with CN-2-Np in the same conditions (Scheme 1), a garnet-red solid resulted by precipitation with acetone, which was identified as a mixture of [Pt(bzq)Cl(CN-2-Np)] **3** and the salt product [Pt(bzq)(CN-2-Np)$_2$]$^+$[Pt(bzq)Cl$_2$]$^-$ **4** (molar ratio ~1:1). In accordance with the formation of **4**, the MALDI-TOF spectrum of the garnet-red solid (mixture of **3** and **4**) showed a cluster of peaks with maximum at *m*/*z* 1089 (Figure 2a), the value and isotropic pattern of which

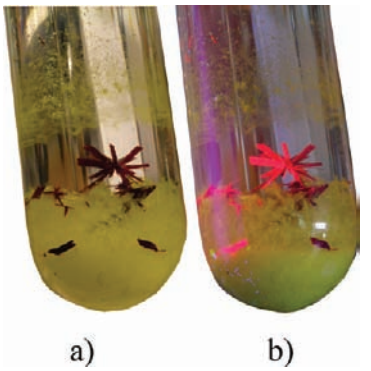

Figure 1. (a) Photographic images of the [Pt(bzq)Cl(CN-^{t}Bu)] yellow [**1**·**0.5H$_2$O**]$_2$ and red [**1**·**CHCl$_3$**]$_\infty$ pseudopolymorphs grown simultaneously from $CHCl_3$/*n*-hexane solution at −30 °C; (b) The same crystals on the left but under UV light (365 nm).

correspond to the {[Pt(bzq)(CN-2-Np)$_2$][Pt(bzq)Cl]}$^+$ species. As shown in Scheme 1, the salt complex **4** was alternatively prepared by mixing an equimolar mixture of [Pt(bzq)(CN-2-Np)$_2$]PF$_6$ and NBu$_4$[Pt(bzq)Cl$_2$] in acetone. For **4**, two characteristic strong ν_{CN} IR absorptions slightly shifted to higher frequencies (2223 and 2192 cm^{-1}) in relation to the precursor [Pt(bzq)(CN-2-Np)$_2$]PF$_6$ (2215, 2189 cm^{-1})[31] are observed. This fact is likely an effect of the lower electron-backdonation to the isocyanides because of the presence in the salt **4** of a Pt···Pt bonding interaction. In solution (CH_2Cl_2, $CHCl_3$) **4** is unstable, evolving to the neutral final isomer **3**, with CN-2-Np *trans* to nitrogen (bzq) (ν_{CN} 2185vs, 2142sh cm^{-1}), as confirmed by X-ray diffraction study (see below). This isomerization takes place through the formation of **3′** (with CN-2-Np *trans* to metalated carbon) as is shown by ^{1}H NMR spectroscopy. As is seen in Supporting Information, Figure S1, the characteristic H^2 signal, which

(58) Jain, V. K.; Jain, L. *Coord. Chem. Rev.* **2005**, *249*, 3075.
(59) Vicente, J.; Arcas, A.; Gálvez-López, M. D. *Organometallics* **2009**, *28*, 3501.

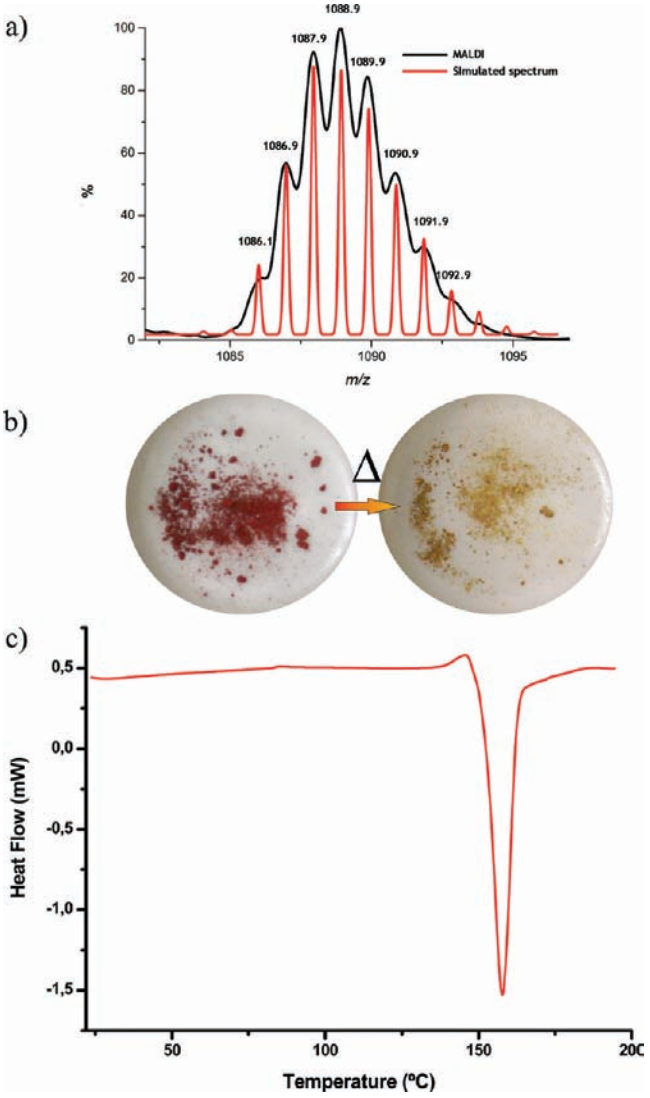

Figure 2. (a) MALDI-TOF spectrum of the garnet-red solid (mixture of **3** and **4**). Peak corresponding to $\{[Pt(bzq)(CN\text{-}2\text{-}Np)_2][Pt(bzq)Cl]\}^+$ $[\mathbf{4} - Cl]^+$ (experimental, black; simulated, red). (b) Photographic images of the transformation of the garnet-red crude solid (mixture of **3** and **4**) to **3** at 150 °C for 1 h. (c) DSC curve of **4** from 25 to 200 °C.

is very sensitive to the stereochemistry around Pt, of **3′** (δ = 9.15, green) and **3** (δ = 9.76, blue) is clearly observed together with those of **4** (δ = 9.38, 9.08, red), 5 min after the first spectrum was run. The signals of **4** disappear after 15 min, but total isomerization to **3** is only complete after 5 days. Interestingly, **3** was also obtained by a thermal (1 h at 150°) irreversible solid-state evolution of the initial mixture of **3** and **4** (1:1) (Figure 2b and Scheme 1). This evolution agrees with the differential scanning calorimetry (DSC) measurement of **4** (Figure 2c), which shows an exothermic peak ($\Delta H = -49 \pm 5$ kJ/mol) at about 152 °C, that can be attributed to the solid−solid transition (red to yellow).

All **1**−**4** complexes were also fully characterized by ^1H and $^{13}C\{^1H\}$ NMR spectroscopy and usual analytical means (details are given in the Supporting Information). For **1**−**3**, crystals suitable for X-ray diffraction were obtained, allowing the determination of their crystal structures. However, all attempts that we made to obtain crystals of **4** suitable for X-ray (monocrystal and powder) were unsuccessful. In this complex, the spectroscopic data and MALDI-TOF spectrum support its formulation as a double salt $[Pt(bzq)(CN\text{-}2\text{-}Np)_2][Pt(bzq)Cl_2]$, most likely stabilized by a polar $Pt^{\ominus}$-$Pt^{\oplus}$ electrostatic attraction, which in its turn would account for this deep garnet-red color. Notwithstanding, the presence of more or less extended chains in the crude solid cannot be excluded.

The molecular structures of **1**−**3** (Figures 3−6, Table 1) confirm that in all cases the isomer generated has the isocyanide ligand *trans* to nitrogen of the bzq group, which is a feature consistent with the *transphobia* effect.[60−62] As commented above, yellow crystals of $[\mathbf{1}\cdot\mathbf{0.5H_2O}]_2$ ($[\mathbf{1}]_2$) and red crystals of $[\mathbf{1}\cdot\mathbf{CHCl_3}]_\infty$ ($[\mathbf{1}]_\infty$) were grown simultaneously by slow diffusion of *n*-hexane into a $CHCl_3$ solution of the orange crude solid **1** at −30 °C. The distinguishing feature of both crystal forms lies in their different packing arrangement. In $[\mathbf{1}\cdot\mathbf{0.5H_2O}]_2$ ($[\mathbf{1}]_2$), the four molecules found in the asymmetric unit are oriented to approximately form a square (Figure 3b), but the molecules are packed by dimers in a head-to-head fashion (Figure 3c, torsion angle ∼23°), stabilized by both close interplanar bzq $\pi\cdots\pi$ interactions [3.3139(1)−3.5795(1) Å],[14,24−27,29,30,63,64] and a short Pt···Pt distance (3.2732(4) Å [Pt(1)−Pt(4′)] and 3.2394(4) Å [Pt(2)−Pt(3′)]). The water molecules are associated to the lattice through weak hydrogen bonding between the oxygen atoms and protons of the two *tert*-butyl groups (O···H of each dimer, 2.66(2), 2.64(2), 2.47(2) Å) (Figure 3c). In contrast, in the crystal packing of $[\mathbf{1}\cdot\mathbf{CHCl_3}]_\infty$ ($[\mathbf{1}]_\infty$) (Figure 4), the [Pt(bzq)Cl(CN-^{t}Bu)] units stack in a columnar way along the *a*-axis with a Cl−Pt−Pt−C_α twist angle of 30.35°, thereby minimizing steric interactions between ^{t}Bu groups and allowing a close proximity of neighboring Pt centers. The extended 1D-chain exhibits equivalent Pt(II)−Pt(II) distances of 3.3547(2) Å and a nearly linear Pt···Pt···Pt angle [169.12(2)°], thus indicating some degree of Pt···Pt interactions along the chain. It is noteworthy that the formation of columnar-stacked chain Pt(II) structures stabilized by Pt···Pt metallophilic interactions is now a well recognized process, and many examples have been reported.[7,20,34,37,49,50,56,65−67] In $[\mathbf{1}]_\infty$, the shortest observed interplanar separation between the bzq ligands [3.349(1) Å] is also sufficiently close to suggest the simultaneous presence of $\pi\cdots\pi$ interactions.[14,24−27,29,30,63,64] The red form ($[\mathbf{1}]_\infty$) appears to pack in such a way as to minimize void space, and this fact is consistent with a higher calculated density of 2.003 g cm^{-1} for $[\mathbf{1}]_\infty$ versus 1.954 g cm^{-1} for $[\mathbf{1}]_2$. The crystal packing is additionally stabilized by intermolecular hydrogen bonds [C−H(solvent)···Cl] ($d_{C-H\cdots Cl}$ = 2.572 Å) between the H atoms of the occluded $CHCl_3$ molecules and the Cl ligand (see Figure 4b). Several

(60) Vicente, J.; Abad, J. A.; Martínez-Viviente, E.; Jones, P. G. *Organometallics* **2002**, *21*, 4454.
(61) Vicente, J.; Arcas, J. A.; Farkland, A. D.; Ramírez de Arellano, M. C. *Chem.—Eur. J.* **1999**, *5*, 3066.
(62) Vicente, J.; Arcas, A.; Gálvez-López, M. D. *Organometallics* **2006**, *25*, 4247.
(63) *Supramolecular Chemistry*; Steed, J. W., Atwood, J. L., Eds.; Wiley-Interscience: Chichester, 2000.
(64) Houlding, V. H.; Miskowski, V. M. *Coord. Chem. Rev.* **1991**, *111*, 145.
(65) *Comprehensive Organometallic Chemistry III*; 3rd ed.; Canty, A., Ed.; Elsevier: Amsterdam, The Netherlands, 2006; Vol. *8*.
(66) Miller, J. S. *Extended linear chain compounds*; Plenum Press: New York, 1982; Vol. *1*−*3*.
(67) Williams, J. M. *Adv. Inorg. Chem. Radiochem.* **1983**, *26*, 235.

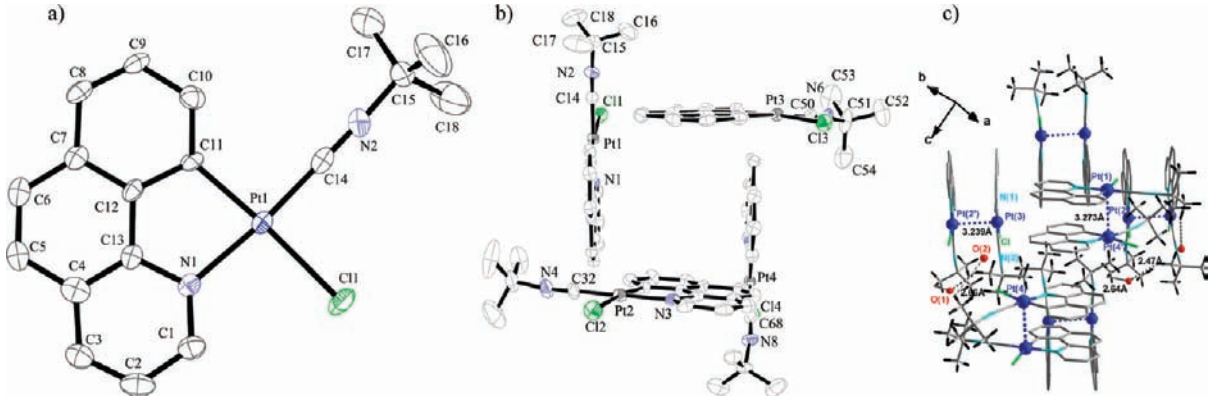

Figure 3. (a) ORTEP drawing of the molecular structure of the monomer in the yellow form ($[\mathbf{1}\cdot 0.5H_2O]_2$). (b) Asymmetric part of the unit cell. Ellipsoids are drawn at the 50% probability level, and hydrogen atoms are omitted for clarity. (c) Crystal packing by dimers. The oxygen atoms for included water molecules are colored red in the diagram.

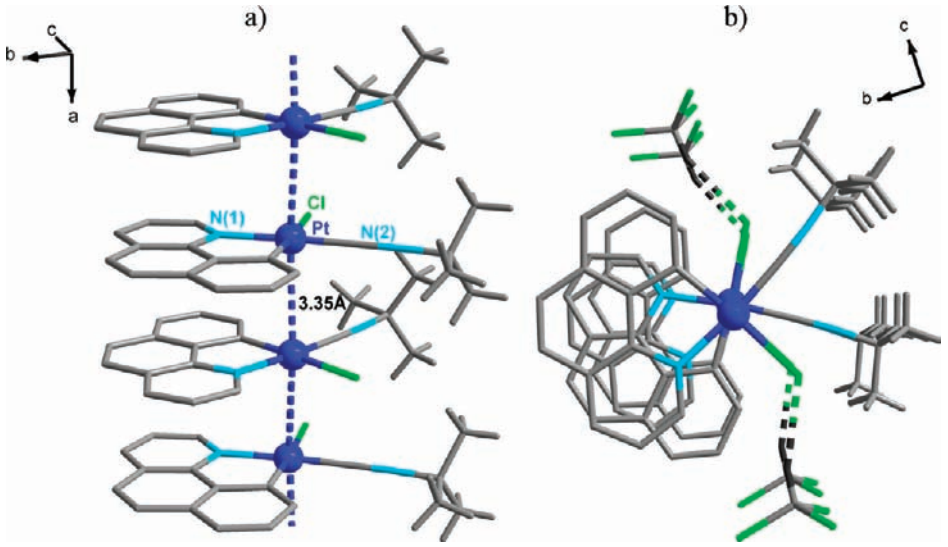

Figure 4. (a). Crystal packing of the red form $[\mathbf{1}\cdot CHCl_3]_\infty$ along *a* axis. (b) View down the *a* axis showing the relative orientation of adjacent [Pt(bzq)Cl(CN-^{t}Bu)] molecules and the interaction between the Cl and $HCCl_3$ molecule.

examples of platinum(II) compounds that exist in two different color forms have been reported.[68]

In the molecular structure of **2** (yellow crystals, Figure 5) there are no metallophilic interactions, probably because of the steric hindrance of the Xyl ring, which is found to form a dihedral angle of 43.80° with the platinum coordination plane. The molecules are oriented in head-to-tail pairs with a short [3.293(8) Å] interplanar separation between the bzq groups (Figure 5b). Curiously, similar arrangements were also found in both yellow cations of $[Pt(bzq)(CN\text{-}Xyl)_2]^+$ with ClO_4^- and PF_6^-.[31] Despite the yellow color of the crystals of the naphthylisocyanide $\mathbf{3}\cdot\mathbf{CH_2Cl_2}$, in this complex the two molecules found in the asymmetric unit (Figure 6a) form a dimer linked by short Pt···Pt [3.1451(8) Å] and $\pi\cdots\pi$ (bzq) [3.340(2) Å] interactions (torsion angle Cl−Pt−Pt−C_α 28.52°). The naphthyl groups are essentially coplanar with the respective platinum planes [dihedral angles 12.23°, Pt(1) and 9.00°, Pt(2)] and this coplanarity favors the existence of an additional stacking pattern (Figure 6b) in which dimers are arranged in close proximity by $\pi\cdots\pi$ interactions [bzq-Np groups 3.271(2)-3.360(2) Å]. The long Pt···Pt distances between dimers [5.056(1) Å and 5.301(1) Å] and torsion angles of 130.57(1)° [Pt(1′)−Pt(1)−Pt(2)] and 129.37(1)° [Pt(2)−Pt(1′)−Pt(2′)] indicate a notable slide from one to another.

Photophysical Properties. Absorption Spectra. Electronic absorption spectra of **1**−**3** are recorded in several solvents with increasing polarity (Toluene, 2-MeTHF, CH_2Cl_2 and MeCN) and the data are summarized in Supporting Information, Table S1. As an illustration, the spectra in CH_2Cl_2 are shown in Figure 7a-c. They reveal several intense absorptions (222 to 340 nm), which were mainly considered to be due to intraligand (^{1}IL, bzq, CNR) and metal perturbed intraligand transitions. The middle absorption envelope in the region 285−340 nm, most likely have contributions from ^{1}MLCT and ^{1}LL′CT transitions, according to DFT calculations (see below). The low energy bands show little dependence on the isocyanide substituent with a slight red-shift on going from **1** to **3** (CH_2Cl_2, 396, 410 **1**; 397, 412 **2**; 398, 414 nm **3**)

(68) Often stacked in the solid state causes intense color and luminescence based on Pt···Pt electronic interactions. A search of the July 2009 version of the Cambridge Structural Database (CSD) indicated the existence of 301 polymorphic or pseudopolymorphic platinum complexes, 13 of which have at least one polymorph with an intermolecular Pt···Pt interaction < 3.5 Å.

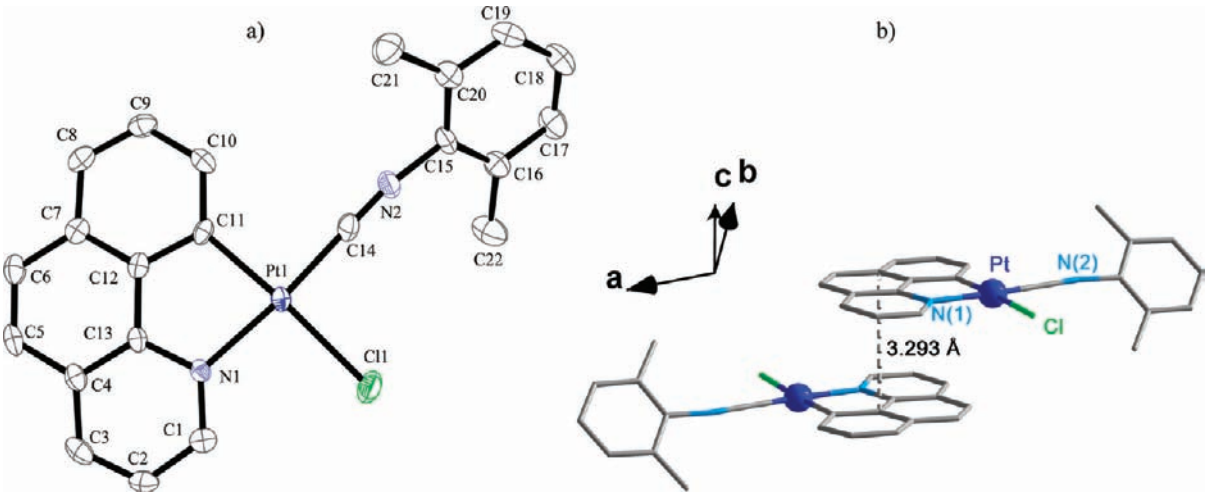

Figure 5. (a) ORTEP drawing of the molecular structure of **2**. Ellipsoids are drawn at the 50% probability level, and hydrogen atoms are omitted for clarity. (b) Crystal packing of **2**.

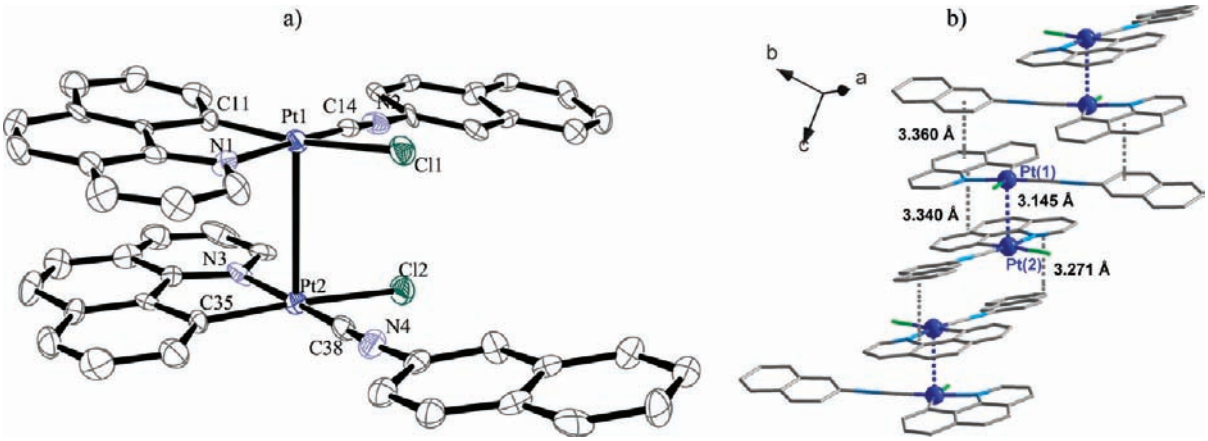

Figure 6. (a) ORTEP drawing of the asymmetric part of $[\mathbf{3}\cdot\mathbf{CH_2Cl_2}]_2$. Ellipsoids are drawn at the 50% probability level, and hydrogen atoms are omitted for clarity. (b) Crystal packing of $[\mathbf{3}\cdot\mathbf{CH_2Cl_2}]_2$.

Table 1. Selected Bond Lengths [Å] and Bond Angles [deg] for $[\mathbf{1}\cdot\mathbf{0.5H_2O}]_2$, $[\mathbf{1}\cdot\mathbf{CHCl_3}]_\infty$, **2**, and $[\mathbf{3}\cdot\mathbf{CH_2Cl_2}]_2$

	$[\mathbf{1}\cdot\mathbf{0.5H_2O}]_2$	$[\mathbf{1}\cdot\mathbf{CHCl_3}]_\infty$	**2**	$[\mathbf{3}\cdot\mathbf{CH_2Cl_2}]_2$
		Distances [Å]		
Pt···Pt	3.2732(4); 3.2394(4)	3.3547(2)		3.1451(8)
Pt−N_{bzq}	2.075(6)	2.049(8)	2.075(4)	2.064(9), 2.090(9)
Pt−C_{orth}	2.011(7)	2.012(10)	1.998(5)	1.972(11), 2.011(11)
Pt−$C_{isocyanide}$	1.896(8)	1.899(12)	1.895(5)	1.913(14), 1.915(11)
$C_{isocyanide}$−$N_{isocyanide}$	1.152(10)	1.147(17)	1.139(7)	1.127(15), 1.130(14)
		Angles [deg]		
N_{bzq}−Pt−C_{orth}	81.5(3)	82.5(4)	81.88(19)	82.4(4), 82.3(4)
Pt−$C_{isocyanide}$−$N_{isocyanide}$	178.7(7)	178.1(13)	179.0(5)	176.4(11), 178.4(12)
$C_{isocyanide}$−Pt−C_{orth}	93.2(3)	92.0(5)	93.1(2)	91.6(4), 93.4(5)
Cl−Pt−N_{bzq}	94.08(17)	93.4(2)	94.19(12)	92.3(3), 92.9(3)

and a modest negative solvatochromism (~12 **1**; 13 nm **2** and **3**) from toluene to MeCN (see Supporting Information, Table S1 and Figure S2a for **3**). These bands are attributed to admixture of intraligand $\pi\rightarrow\pi^*$ (bzq) ^{1}IL and metal-to-ligand [dπ(Pt)$\rightarrow\pi^*$(bzq)] ^{1}MLCT and [dπ(Pt)$\rightarrow\pi^*$(CNR)] ^{1}ML′CT states, respectively, with the metal-to-isocyanide charge transfer increasing from **1** to **3**, as supported from DFT calculations. For all three complexes, the lowest absorption band (410−414 nm) follows the Beer's law in the concentration range from 5×10^{-5} M to 10^{-3} M (see Supporting Information, Figure S2b,c for **3**), suggesting that no obvious aggregation occurs within this range. However, a very weak absorption [ε(M^{-1} cm^{-1}) ~2.4 **1** < 3.2 **2** < 6.1 **3**] at a longer wavelength (~465 nm), is discernible in very concentrated solutions (10^{-2} M, Supporting Information, Figure S2d for **3**). This band could be attributed to the direct population of a triplet state, following previous assignments in

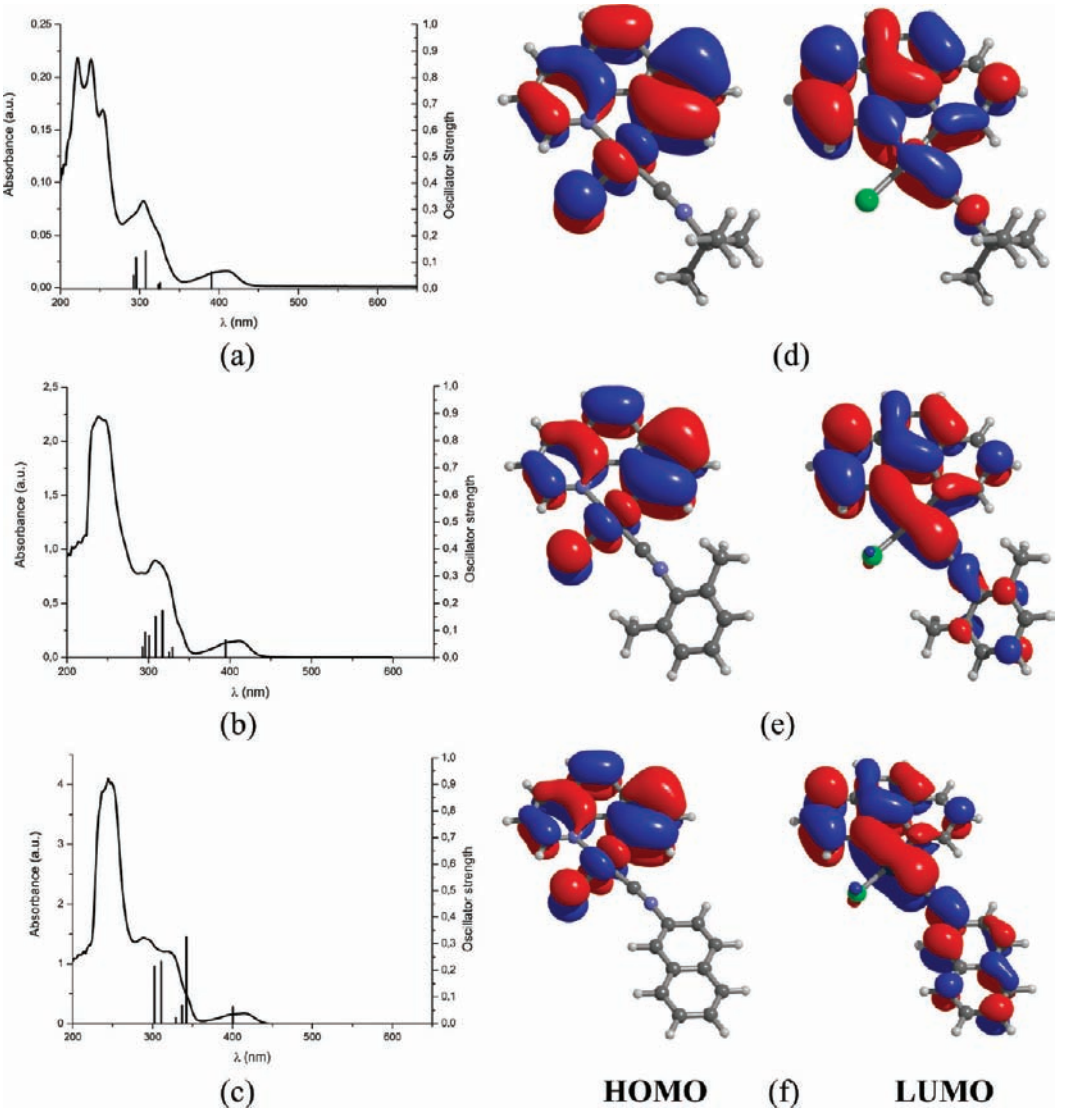

Figure 7. Experimental UV−vis spectra in CH_2Cl_2 (5×10^{-5} M) at 298 K and calculated absorption spectra (bars) in CH_2Cl_2 of **1** (a), **2** (b), and **3** (c). Frontier orbital plots for **1** (d), **2** (e), and **3** (f) obtained by DFT.

Pt(II) cromophores;[24,27−29,31,69,70] however, in these complexes the formation of aggregates in some extent cannot be excluded.

Interestingly, although the yellow crystals of $[\mathbf{1}]_2$, **2**, and **3** form dimers with short $\pi\cdots\pi$ and/or Pt···Pt distances, these are not reflected in their solid diffuse reflectance UV−vis spectra (Supporting Information, Table S1 and Figure 8 for $[\mathbf{1}]_2$), which are similar to those seen in solution, probably because they are not of a long-range. By contrast, the 1-D extended red form $[\mathbf{1}]_\infty$ displays the expected distinctive very low feature at 560 nm (Figure 8) ascribed to a ^{1}MMLCT [d(σ^*)→ $\sigma(\pi^*)$] transition likely with a slight intraligand $^1[\sigma^*(\pi)\rightarrow\sigma(\pi^*)]$ contribution. As seen in Figure 8, the low energy absorption profile of the crude orange **1** (λ_{max} 480 nm) lies between those of $[\mathbf{1}]_2$ (short-range interactions) and $[\mathbf{1}]_\infty$ (long-range interactions). In support of the formulation proposed, the garnet double-salt **4** also shows a distinct ^{1}MMLCT strong broad band at 520 nm (Supporting Information, Figure S3).

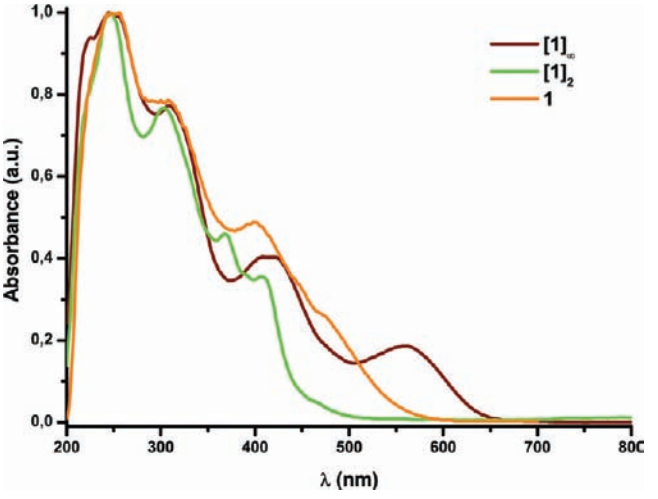

Figure 8. Normalized absorption spectra calculated from their reflectance spectra of **1**, $[\mathbf{1}]_2$, and $[\mathbf{1}]_\infty$ in solid state.

(69) Berenguer, J. R.; Lalinde, E.; Torroba, J. *Inorg. Chem.* **2007**, *46*, 9919.
(70) Develay, S.; Blackburn, O.; Thompson, A. L.; Williams, J. A. G. *Inorg. Chem.* **2008**, *47*, 11129.

Table 2. Photophysical Data for **1**−**4**

compound	media (T/K)	λ_{em} [nm]	τ [μs]
1 orange	solid (298)	a	
	solid (77)	595 (λ_{ex} 400)	11.8
$[\mathbf{1}]_2$ yellow form	yellow crystals (77)	535_{max}, 600_{sh} (λ_{ex} 400)	66.2 (535)
$[\mathbf{1}]_\infty$ red form	red crystals (298)	672 (λ_{ex} 500−600)[b]	
	red crystals (77)	744 (λ_{ex} 590)[b]	
	CH_2Cl_2 5×10^{-5} M (298)	350_{max}, 366, 385, 473, 500, 542 (λ_{ex} 310)	
		473_{max}, 505, 542 (λ_{ex} 400)	0.2 (473)
	CH_2Cl_2 5×10^{-5} M (77)	475, 510, 560_{max} (λ_{ex} 400)	21.5 (560)
		560, 640 (λ_{ex} 480)	
	CH_2Cl_2 10^{-3} M (77)	560 (λ_{ex} 400)	24.0 (560)
		560, 640_{max} (λ_{ex} 470)	14.6 (640)
2	solid (298)	485_{sh}, 508_{max}, 545, 600_{sh} (λ_{ex} 400)	12.4 (508)
			10.7 (89%), 38.9 (11%) (545)
	solid (77)	505_{max}, 545_{max}, 580, 630_{sh} (λ_{ex} 400)	87.3 (82%), 265 (18%) (505)
			88.3 (80%), 301 (20%) (545)
	CH_2Cl_2 5×10^{-5} M (298)	350, 370, 385, 473_{max}, 505, 540_{sh} (λ_{ex} 315)	0.2 (350); 0.2 (473)[c]
		473_{max}, 505, 540_{sh} (λ_{ex} 415)	
	CH_2Cl_2 5×10^{-5} M (77)	490, 570_{max} (λ_{ex} 320)	80.1 (60%), 460 (40%) (490)
		490, 540, 620_{max} (λ_{ex} 400)	19 (60%), 117 (40%) (570)
			28.3(60%), 128 (40%) (620)
	CH_2Cl_2 10^{-3} M (298)	473_{max}, 505, 540_{sh}, 585, 695(λ_{ex} 436)	82 ns(473), 0.8 (585), 0.3 (695)
		585, 695_{max}(λ_{ex} 464)	
	CH_2Cl_2 10^{-3} M (77)	550_{sh}, 600−620_{max} (λ_{ex} 360−450)	
		685_{max} (λ_{ex} 500)	2.2 (685)
3	solid (298)	non-emissive	
	solid (77)	533_{max}, 570, 615_{sh} (λ_{ex} 400−460)	33.1 (88%), 152 (12%) (533)
	CH_2Cl_2 5×10^{-5} M (298)	350_{max}, 365, 385, 475, 490, 500, 525_{sh} (λ_{ex} 330)	
		475, 490_{max}, 501, 525_{sh} (λ_{ex} 400)	0.1 (475)[c]
	CH_2Cl_2 5×10^{-5} M (77)	490, 500, 570_{max}, 680 (λ_{ex} 415)	1.8 (570)
		680_{max} (λ_{ex} 490)	
	CH_2Cl_2 10^{-3} M (298)	350, 366_{max}, 385 (λ_{ex} 300−320)	
		440, 474_{max}, 490, 500, 522_{sh}, 575_{sh} (λ_{ex} 370)	
		474_{max}, 490, 500, 522_{sh}, 575_{sh} (λ_{ex} 430)	
		550_{max}, 585_{sh} (λ_{ex} 480)	
	CH_2Cl_2 10^{-3} M (77)	490, 500, 580_{max} (λ_{ex} 330)	1.7 (580)
		706 (λ_{ex} 480)	2.5 (706)
4[d]	solid (298)	680 (λ_{ex} 500−600)	e
	solid (77)	675, 730_{max} (λ_{ex} 500)	e

[a] Weak emission at 590 nm (λ_{ex} 440 nm). [b] In atmosphere totally exempt of humidity (see text). [c] See study of the dependence of the τ_{obs} versus [Pt] in text. [d] **4** evolves to **3** in solution in about 30 min. [e] Too weak to be measured.

Emission Spectroscopy. Solid State. The photophysical data are summarized in Table 2 and Supporting Information, Table S2. Powdered orange samples of **1** are only weakly emissive at 298 K, showing an emission peak at about 590 nm, which is visibly more intense at 77 K (λ_{max} 595 nm, τ = 11.8 μs) (Figure 9). Crystalline yellow form $[\mathbf{1}\cdot\mathbf{0.5H_2O}]_2$ ($[\mathbf{1}]_2$) is not emissive at 298 K, but displays a bright green-yellow unsymmetrical broad emission (λ_{max} 535 nm, tailing to 725 nm) with a relatively long lifetime of 66.2 μs at 77 K. The lack of a clear vibronic structure suggests that the emission is unlikely to be ^{3}IL.[64,71] The broad shape and the time-resolved phosphorescence measurements (Supporting Information, Figure S4) are consistent with an only emission band, which is tentatively assigned as ^{3}MLCT phosphorescence. In this form, the H_2O molecules are well trapped, and all attempts to dry it under vacuum or by heating without decomposition were unsuccessful. The crystalline red form ($[\mathbf{1}]_\infty$) exhibits, in a dry atmosphere under argon at 298 K, a structureless emission centered at 672 nm, which narrows and considerably shifts to lower energies (λ_{max} 744 nm, λ_{exc} 590 nm) at 77 K (Figure 9). In conjunction with the observed Pt···Pt and $\pi\cdots\pi$ contacts in its crystal structure and recent theoretical calculations on Pt···Pt bonding systems,[72−74] the emission is assigned, as in other stacked platinum chain systems,[7,50,64,75−78] to mixed ^{3}MMCT [d(σ*)→p(σ)] and ^{3}MMLCT [dσ*$(M)_2$→$\sigma(\pi^*)$(C^N)] transitions. We observed that the crystalline red form ($[\mathbf{1}]_\infty$) lost its shine very quickly, and this was followed by a gradual change in its color and emissive behavior (Figure 10). In fact, the emission spectrum of $[\mathbf{1}]_\infty$ at 77 K in air exhibits the expected band at 744 nm together with a small high-energy shoulder at 640 nm (orange line in Figure 10). In a few minutes (10 min) this shoulder grows and a new high-energy feature located at 590 nm is also detected upon excitation at 500 nm. The relative intensities of the three bands depend on the

(71) Kui, S. C. F.; Sham, I. H. T.; Cheung, C. C. C.; Ma, C. W.; Yan, B.; Zhu, N.; Che, C. M.; Fu, W. F. *Chem.—Eur. J.* **2007**, *13*, 417.

(72) Aullón, G.; Alvarez, S. *Chem.—Eur. J.* **1997**, *3*, 655.

(73) Xia, B. H.; Che, C. M.; Phillips, D. L.; Leung, K. H.; Cheung, K. K. *Inorg. Chem.* **2002**, *41*, 3866–3875.

(74) Koo, C. K.; Wong, K. L.; Lan, K. C.; Wong, W. Y.; Lam, M. H. W. *Chem.—Eur. J.* **2009**, *15*, 7689.

(75) Kato, M.; Kosuge, C.; Morii, K.; Ahn, J. S.; Kitagawa, H.; Mitani, T.; Matsushita, M.; Kato, T.; Yano, S.; Kimura, M. *Inorg. Chem.* **1999**, *38*, 1638.

(76) Kato, M.; Kishi, S.; Wakamatsu, Y.; Sugi, Y.; Osamura, T.; Koshiyama, M.; Hasegowa, M. *Chem. Lett.* **2005**, *34*, 1368.

(77) Connick, W. B.; Henling, L. M.; Marsh, R. E.; Gray, H. B. *Inorg. Chem.* **1996**, *35*, 6261.

(78) Bailey, J. A.; Hill, M. G.; Marsh, R. E.; Miskowski, V. M.; Schaefer, W. P.; Gray, H. B. *Inorg. Chem.* **1995**, *34*, 4591.

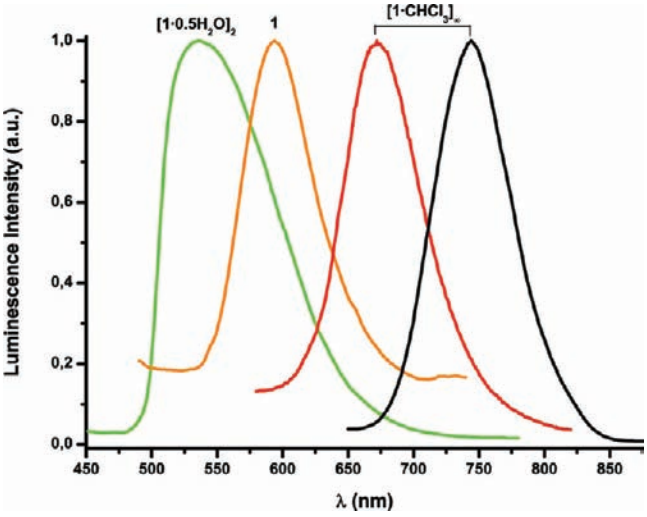

Figure 9. Normalized emission spectra of the crude solid **1** (77 K, λ_{exc} 400 nm), of the yellow crystalline form $[\mathbf{1}\cdot\mathbf{0.5H_2O}]_2$ (77 K, λ_{exc} 400 nm) and of the red crystals $[\mathbf{1}\cdot\mathbf{CHCl_3}]_\infty$ (measured under Ar: red 298 K, λ_{exc} 500 nm; black 77 K, λ_{exc} 590 nm).

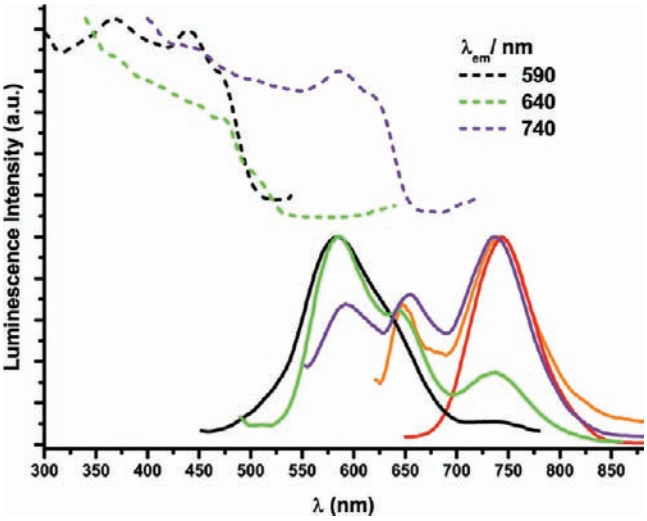

Figure 10. Normalized excitation (top) and emission (down) spectra of red crystals of $[\mathbf{1}\cdot\mathbf{CHCl_3}]_\infty$ in the solid state at 77 K: fresh crystals under Ar (Red, λ_{exc} 590 nm); under air for 2 min (Orange, λ_{exc} 500 nm); upon exposure to standard conditions for 10 min (Green, λ_{exc} 450 nm; Blue, λ_{exc} 500 nm) or for 4 days, λ_{exc} 400 nm (Black).

excitation wavelength (green and blue lines in Figure 10), and the corresponding excitation spectra are different, thus suggesting a different origin of these bands (Figure 10, top). The color of the sample gradually changes from red to orange, and finally on standing for 4 days, an orange-ochre powder is obtained. This final solid is not emissive at room temperature, whereas at 77 K it mainly shows the high-energy emission band located at ~590 nm, similar to that seen in crude solid **1** at 77 K (595 nm) (black line in Figure 10). We suggest that the behavior observed arises most likely from the fact that the initial loss of crystallization solvent ($CHCl_3$) causes a disruption of the lattice and presumably a modification of the stacking. A change from the initial nearly linear Pt−Pt−Pt chain (~170°) to a more slip-stacked (Pt−Pt−Pt < 170°, or even more staggered) could result in a lengthening of the Pt−Pt separation, explaining the change from red to orange and the emission at about 640 nm. In the final orange-ochre powder, the $\pi\cdots\pi$ stacking between units is likely prevalent and responsible for the unstructured emission at about 590 nm. The modification of the photophysical properties (vaprochromism and/or vapoluminescence, excimer generation) caused by structural rearrangements upon exposure of platinum linear chain materials to solvents or by simple grinding has now many precedents.[7,37,50,79−81] However, the observed change is not reversible, because when the final orange-ochre powder is exposed to $CHCl_3$ vapors, we observed neither its transformation to the red form nor any modification in the emission spectra.

Complex **2** in crystalline state at 298 K exhibits a broad structured green emission (λ_{max} 508 nm), which is slightly blue-shifted at 77 K (505 nm) (Supporting Information, Figure S5). In contrast, **3** in solid state is only emissive at 77 K displaying the typical structured band (λ_{max} 533 nm) due to the monomer. For both complexes the relatively long lifetimes, which fit to two components (see Table 2), suggest that the emission can be assigned to combined ^{3}LC and ^{3}MLCT transitions. The salt **4** displays a characteristic low energy ^{3}MMLCT emission band at 680 nm (λ_{exc} 500−600 nm) in the solid state at 298 K, which, as expected, red shifts to 730 nm upon cooling to 77 K (Supporting Information, Figure S6).

Solution and Glass State. Complexes **1**−**3** are emissive in solution at 298 K (see Table 2, Supporting Information, Table S2, Figure 11, and Supporting Information, Figures S7−S9). In diluted (5×10^{-5} M) CH_2Cl_2 solutions they all exhibit fluorescence from the bzq ligand $^1(\pi\pi^*)$ (350−425 nm) together with a vibronic structured emission at 473−540 nm, upon excitation in the 290−330 nm range (Figure 11 solid lines and time-resolved spectra for **2** in Supporting Information, Figure S7,[82]). As expected, excitation at their lowest energy absorption (400−415 nm) only results in the corresponding low energy vibronic band (dashed lines), whose excitation spectrum resembles the absorption spectrum. For **1** and **2**, the peak maxima (~473, 505, 540 nm), and lifetimes are nearly coincident, indicating a rather similar emissive state. Only minor differences are found when compared with the cationic derivatives $[Pt(bzq)(CNR)_2]^+$ (CH_2Cl_2, 470 nm R = ^{t}Bu; 476 nm R = Xyl).[31] For **3**, with the most conjugated and electron-withdrawn ligand (CN-2-Np), the emission profile is slightly red-shifted and more complex (475, 490, 500, 525 nm) having an additional peak maximum at 490 nm, pointing to a different composition of the low-lying emitting state. The phosphorescent emission is ascribed in the three complexes (**1**−**3**) mainly as intraligand charge transfer ^{3}ILCT on the benzoquinolinate ligand, mixed with some ^{3}MLCT/^{3}ML′CT (L = bzq, L′ = CNR) character, with the contribution of the

(79) Wadas, T. J.; Wang, Q. M.; Kim, Y. J.; Flaschenreim, C.; Blanton, T. N.; Eisenberg, R. *J. Am. Chem. Soc.* **2004**, *126*, 16841.
(80) Balch, A. L. *Angew. Chem., Int. Ed.* **2009**, *48*, 2641.
(81) Abe, T.; Itakura, T.; Ikeda, N.; Shinozaki, K. *Dalton Trans.* **2009**, 711.

(82) For **2**, which exhibited the more intense emission, time-resolved emission in the millisecond time scale was examined, showing a similar decay for the fluorescence and the phosphorescence, indicating that delayed fluorescence is present, a feature which has precedents in alkynyl platinum complexes. See: Bellows, D.; Aly, S. M.; Gros, C. P.; Ojaimi, M. E.; Barbe, J. M.; Guilard, R.; Harvey, P. D. *Inorg. Chem.* **2009**, *48*, 7613.

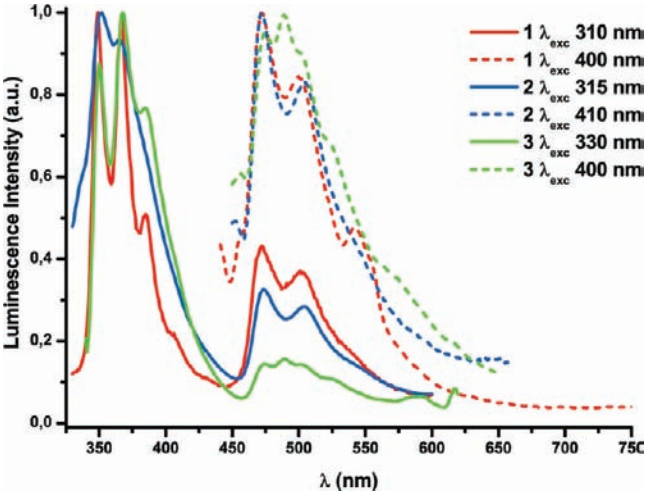

Figure 11. Normalized emission spectra of **1**−**3** in CH_2Cl_2 (5×10^{-5} M) at 298 K.

isocyanide (L′) being minimal in **1** and maximum in **3**, as supported by DFT studies.

The occurrence of low-energy emission, usually ascribed to excimers or aggregates, is frequently encountered in some Pt(II) complexes;[7,14,21−24,26−31,83] therefore, the influence of the concentration was examined. The emission profile is independent of complex concentration (down 10^{-3} M for **1** and 10^{-4} M for **2** and **3**). In more concentrated solutions (10^{-4} to 10^{-3} M), two small low energy broad bands at ∼585 and 695 nm were observed for **2**, in addition to the structured band around 475 nm (Supporting Information, Figure S8). Similar excitation spectra were obtained for the intermediate (∼585 nm) and the monomer structured band (475 nm), which are consistent with excimer emission. By contrast, the excitation profile of the lowest energy band (695 nm) is red-shifted, therefore, being tentatively ascribed to intermolecular aggregation. At 10^{-3} M, compound **3** shows (Supporting Information, Figure S9), in addition to the $^1\pi\pi^*$ fluorescence (λ_{max} 350 nm, λ_{exc} < 320 nm) and the structured band associated with the monomer (474−490 nm), two new bands centered at about 440 nm and at 550 nm, respectively. The unstructured band at 440 nm, which is related to an excitation maximum at 370 nm and a shoulder at about 350 nm, is tentatively ascribed, as in $[Pt(bzq)(CNR)_2]Q$,[31] to excimer fluorescence. However, the excitation profile of the low-energy emission (550 nm) differs from that of the monomer emission, suggesting that this likely results from intermolecular $\pi\cdots\pi$ aggregation.

Investigation of the dependence of the emission lifetime (τ_{obs}) on the concentration for **2** and **3** indicates that the lifetimes decrease slightly in the 10^{-5} to 2×10^{-4} range from 0.16 to 0.14 μs for **2** and 0.14 to 0.12 μs for **3** (Supporting Information, Figure S10). The estimated values of τ_0 [160 ns (**2**) and 137 ns (**3**)] and the self-quenching constants [6.2×10^9 M^{-1} s^{-1} (**2**) and 4.23×10^9 M^{-1} s^{-1} (**3**)] obtained from extrapolation of the Stern−Volmer plot[84] are in line with those reported for related Pt(II) complexes.[70,85−88]

Even in diluted glassy CH_2Cl_2 solutions (77 K), all complexes exhibit broad low energy emissions (560 **1**, 620 **2** and 570, 680 nm **3**) in addition to the structured monomer emission band (λ_{max} 475 **1**, 490 nm **2**, **3**) (Supporting Information, Figure S11). The excitation spectra monitoring the low energy band at around 570 nm for **1** and **3** and ∼620 nm for **2** closely resemble their UV absorptions (∼400 nm), which is consistent with excimer emission. We suggest that the red-shift observed for this emission in **2** could be related to the different nature of the interaction (bzq-aryl or aryl−aryl) between the excited monomer and the adjacent molecule. In fact, with excitation at higher energies, in the region of intraligand transitions (320 nm), the excimer band in **2** also maximizes at 570 nm (see Supporting Information, Figure S12). However, the lowest energy feature centered at 680 nm in **3** is related to a lower energy excitation profile (∼490 nm), being therefore ascribed to mixed $^3\pi\pi^*/^3$MMLCT transitions from aggregates formed in the rigid matrix at 77 K. Excimeric emission and emission from aggregates ($^3\pi\pi^*/^3$MMLCT) are predominant at higher concentration (10^{-3} M) and the observed maxima (∼560, 640 nm **1**; 600−620, 685 nm **2**; and 580, 706 nm **3**) (Supporting Information, Figure S13) compare well with previously reported values.[83] The emission energy of the lowest band follows the order: R = ^{t}Bu **1** 640 nm > Xyl **2** 685 nm > 2-Np **3** 706 nm, probably because of the formation of dimers or aggregates with decreasing Pt−Pt distances in the same order. In fact, the shortest Pt−Pt (or $\pi\cdots\pi$) distance in the crystal structures has been found in complex **3** [3.1451(8) Å **3** vs 3.2394(4), 3.2732(4) Å $[\mathbf{1}]_2$ or 3.3547(2) Å $[\mathbf{1}]_\infty$].

A solvent-dependent emission study was carried out at 298 K and at 77 K in diluted deoxygenated solutions (5×10^{-5} M) (toluene, 2-MeTHF, and CH_3CN), the results of which are shown in Supporting Information, Table S2. At 298 K, complex **1** only exhibits a fluorescence band (345−408 nm), whereas **2** and **3** exhibit fluorescence and relatively weak phosphorescence without any appreciable energetic variation to their maxima in relation to CH_2Cl_2 (see Supporting Information, Table S2 and Table 2). Only **2** shows one additional low energy (∼580 nm) manifold in CH_3CN. In glassy state, **1** shows ^{3}LC phosphorescence (λ_{max} 474 nm in all solvents) and also a low excimeric manifold (∼570 nm) in CH_3CN. For complexes **2** and **3** (77 K) the tendency to form excimers and/or aggregates is higher. For **2**, monomer emission, [471 nm (toluene), 466 nm (2-MeTHF), 476 nm (CH_3CN)] and broad red features [∼600 nm (toluene); 570, 620 nm (2-MeTHF); 605, 710 nm (CH_3CN)] are seen in all solvents. Similarly, **3** also exhibits multiple structured emissions with several maxima (λ_{max} 478−550 nm) and low energy features [∼590 max, ∼610 nm (toluene and 2-MeTHF); 590, 690 nm (CH_3CN)], which are found to be predominant in the most polar solvent (CH_3CN).

(83) Kim, D.; Brédas, J. L. *J. Am. Chem. Soc.* **2009**, *131*, 11371.
(84) The concentration dependence was expressed by the formula $1/\tau_{obs} = 1/\tau_0 + K_Q[Pt]$, where τ_0 is the lifetime at infinite dilution and K_Q corresponds to the self-quenching constant.
(85) Farley, S. J.; Rochester, D. L.; Thompson, A. L.; Howard, J. A. K.; Williams, J. A. G. *Inorg. Chem.* **2005**, *44*, 9690.
(86) Connick, W. B.; Geiger, D.; Eisenberg, R. *Inorg. Chem.* **1999**, *38*, 3264.
(87) Guo, F.; Sun, W.; Liu, Y.; Schanze, K. *Inorg. Chem.* **2005**, *44*, 4055.
(88) Williams, J. A. G.; Beeby, A.; Davies, E. S.; Weinstein, J. A.; Wilson, C. *Inorg. Chem.* **2003**, *42*, 8609.

TD-DFT Calculations. To further understand the low energy absorption and emission characters of these complexes in CH_2Cl_2, a theoretical investigation was undertaken using the Time-Dependent Density Functional Theory (TD-DFT). Complexes **1**−**3** were first fully optimized in the gas phase using the B3LYP method with the LanL2DZ basis set for Pt and the 6-31G(d,p) basis set for the ligand atoms. The optimized S_0 structures are depicted in Supporting Information, Figures S14−S16, the optimized coordinates for S_0 state in Supporting Information, Tables S3, S5, and S7, and the main geometrical parameters, which are comparable to experimental values, are tabulated in Supporting Information, Table S9. The absorption spectra in CH_2Cl_2 solution for **1**−**3** were explored using the polarizable continuum model, in which the solvent is simulated as a continuum of uniform dielectric ε. The corresponding molecular orbitals (electronic density diagrams) involved in the main excited states have been drawn in Supporting Information, Figures S17−S19, and their relative composition in terms of composing fragments are reported in Table 3. The main conclusion of the frontier orbitals analysis is that the contribution of the CNR ligands increases on going from **1** to **3** as the π-conjugation of the R group increases. Thus, the highest occupied molecular orbitals (HOMOs, Figure 7d−f) are of $\pi^*\{d_\pi(Pt)$-$\pi^*(bzq)$-p(Cl)$\}$ character deriving from a similar configuration of the Pt center (∼20%), bzq ligand (∼72%) and Cl^- (∼8%) in the three complexes. However, whereas the H-1 is also mainly localized on the bzq (90%) in **1**, the participation of the isocyanide ligand increases in **2** (21% CN-Xyl), being clearly predominant in **3** (93% CN-2-Np). With respect to the lowest unoccupied molecular orbitals (LUMOs), they are composed of the bzq ligand (90% **1**, 81% **2**; 63% **3**) with a small contribution of Pt (dπ) (5% 1; 6% **2**; 7% **3**) and isocyanide ligand, which increases from **1** (4%) to **3** (29%). The L+1 is similar to LUMO in **1**, but for **2** and **3**, the contribution of the isocyanide ligand is still higher (29% CN-Xyl **2**; 57% CN-2-Np **3**). Supporting Information, Table S10 shows the calculated excited states in CH_2Cl_2 solution (first singlets) with the oscillator strengths and the transitions with the greatest contributions. Figure 7a−c depicts the selected allowed transitions as bars with the experimentally measured absorptions spectra in CH_2Cl_2. As seen in Supporting Information, Table S10, the dipole-allowed lowest-lying absorptions are at 391, 395, and 400 nm for **1**, **2**, and **3**, respectively, which reproduce, with some blue shifts, the trend observed in the experimental spectra (∼410 **1**, 412 **2**, 414 nm **3**). The major contribution to this band is the HOMO→LUMO transition (95% **1**; 93% **2**, **3**); therefore, the lowest-lying absorption is attributed to the combined transitions of ^{1}ILCT and ^{1}MLCT/^{1}ML′CT (L = bzq; L′ = CNR), with this latter increasing from **1** to **3**. Calculations indicate that there is considerable orbital mixing for the rest of the transitions located at higher energies (λ < 300 nm). A plausible assignment for the remaining calculated transitions, taking into account the nature of the orbitals involved, is included in the Supporting Information, Table S10.

The nature of the low-lying phosphorescent emissions for **1**−**3** in CH_2Cl_2 was also addressed by optimization of the first triplet state (T_1) (Supporting Information, Tables S4, S6, and S8). For comparison with S_0, the structural results are presented in Supporting Information, Table S9. According to TD-DFT calculations, the lowest-energy emissions in CH_2Cl_2 solution are rather similar for the three complexes (533 **1**, 534 **2**, and 532 nm **3**), which are slightly red-shifted in relation to those experimentally observed (λ_{em} 473 **1**, 473 **2**, and 475 nm **3**). A first approach is that the lowest energy phosphorescent emission arises from the singly occupied molecular orbital (SOMO) to the SOMO-1. Inspection of the two SOMOs of the T_1 reveals that the SOMO-1 is similar in the three complexes and resembles the HOMO of the ground state, being mainly contributed from the bzq and d(Pt) components (81% bzq, 16% Pt, 3% Cl). The initial orbital (SOMOs) is mainly localized on the bzq ligand (89% **1**, 86% **2**, 83% **3**) with small contribution of Pt (7%) and the isocyanide ligand (3% **1**, 7% **2**, 9% **3**). Although the contribution of the CNR ligand decreases in relation to the LUMOs in the ground state, its participation in the remaining minor contributions to the lowest phosphorescent emission also increases from the *tert*-butyl (**1**) to the naphthylisocyanide (**3**) derivative. This fact is also illustrated on the more rigorous diagrams of the single-electron transitions, based on the TD-DFT calculation, which are collected in Supporting Information, Figures S20−S22. On the basis of these results, the phosphorescent emission in CH_2Cl_2 solution for **1**−**3** has mainly ^{3}ILCT character located on the cyclometalated ligand perturbed by metal to ligand charge transfer ^{3}MLCT/^{3}ML′CT (L = bzq; L′ = CNR) with the contribution of the isocyanide increasing from **1** (CN^{t}Bu) to **3** (CN-2-Np).

Table 3. Composition (%) of Frontier MOs in the Ground State for **1**−**3** in CH_2Cl_2 Solution

	1				**2**				**3**			
MO	CN-^{t}Bu	Pt	bzq	Cl	CN-Xyl	Pt	bzq	Cl	CN-Np	Pt	bzq	Cl
L+3	18	46	27	8	24	35	36	6	84	3	13	0
L+2	20	15	64	0	49	4	47	0	17	3	80	0
L+1	2	6	92	0	29	7	64	0	57	4	40	0
LUMO	4	5	90	0	13	6	81	0	29	7	63	0
HOMO	0	21	71	8	0	20	72	7	0	20	73	7
H-1	1	7	90	1	21	13	65	1	93	5	2	0
H-2	0	93	6	1	18	64	17	1	12	7	80	1
H-3	0	21	49	29	38	39	21	2	0	92	6	1
H-4	2	22	5	71	92	2	1	5	76	9	15	0
H-5	13	57	25	4	2	22	46	30	2	23	46	30

Conclusion

A new family of isocyanide-cyclometalated platinum complexes **1**−**3** has been prepared and structurally and photophysically characterized. This study shows that the *tert*-butylisocyanide complex **1** co-crystallizes in two pseudopolymorphs: a red form $[\mathbf{1\cdot CHCl_3}]_\infty$, which possesses an infinite 1-D chain network and a yellow form generated by discrete dimers $[\mathbf{1\cdot H_2O}]_\mathbf{2}$. Curiously, although both forms are stabilized by interplanar $\pi\cdots\pi$ and short Pt$\cdots$Pt bonding interactions, only the extended red form $[\mathbf{1\cdot CHCl_3}]_\infty$ shows the characteristic low energy absorption (560 nm) and emission features (672 nm, 298 K; 744 nm 77 K), typical of mixed MMCT [d(σ^*)→p(σ)] and MMLCT [dσ^*(M$_2$)→$\sigma(\pi^*)$(bzq)] transitions. Crystalline state $[\mathbf{1\cdot CHCl_3}]_\infty$ is unstable in the air, likely because of the loss of $CHCl_3$ solvent, evolving irreversibly to an orange-ochre solid, whose photophysical

properties are similar to those of the crude solid **1**. The molecules in [Pt(bzq)Cl(CN-Xyl)] **2** and [Pt(bzq)Cl(CN-2-Np)] **3** arrange in $\pi\cdots\pi$ (bzq) (**2**) and Pt$\cdots$Pt (**3**) contacting dimers, which are found to exhibit typical mononuclear ^{3}LC/^{3}MLCT emissions. Interestingly, the yellow derivative **3** was found to be generated through the garnet-red salt isomer [Pt(bzq)Cl_2][Pt(bzq)(CN-2-Np)$_2$] **4**, which displays a low energy emission arising from a ^{3}MMLCT excited state.

The solution (CH_2Cl_2) absorption and emission properties of **1**−**3** were reasonably elucidated and well supported by TD-DFT calculations. The low energy absorption bands are assigned to an admixture of intraligand $\pi\rightarrow\pi^*$ (bzq) (IL) and metal-to-ligand [dπ(Pt)$\rightarrow\pi^*$(bzq)] MLCT and [dπ(Pt)$\rightarrow\pi^*$(CNR)] ML′CT transitions, with the metal-isocyanide charge transfer growing from **1** to **3**. In fluid diluted solutions, these complexes display both intraligand (bzq) fluorescence and monomer phosphorescence. Their phosphorescence originates from mixed intraligand charge transfer on the cyclometalated ligand ^{3}ILCT [$\pi\rightarrow\pi^*$ (bzq)] and metal-to-ligand (L = bzq, L′ = CNR) charge transfer excited states (^{3}MLCT/^{3}ML′CT) with the Pt$\rightarrow$isocyanide CT contribution increasing from **1** to **3**. Low-energy emissions due to excimer formation and/or ground-state aggregates occur in concentrated ($> 10^{-4}$ M) solutions for **2** and **3** and for all complexes in glass state (77 K) not only in CH_2Cl_2 but also in other solvents (Toluene, 2-MeTHF, CH_3CN), probably facilitated by the presence of aromatic groups and/or Pt(II)$\cdots$Pt(II) interactions as well as by their relatively long lifetimes. Excimeric emission occurs around 560−580 nm, even in diluted glasses, whereas emission from aggregates appears at longer wavelengths in the order 640 nm ^{t}Bu **1** > 685 nm Xyl **2** > 706 nm Np **3**, and is predominant in concentrated (10^{-3} M) solutions.

These results demonstrate the impact of the electronic effects and steric requirements of the CNR ligand, not only in the formation of complexes **1**−**4** but also in their crystal packing through short or long-range Pt$\cdots$Pt and/or $\pi\cdots\pi$ interactions, which have a remarkable role in their photophysical properties. The judicious selection of the CNR ligands, in which the R substituent can be widely modified, could readily lead to remarkable tuning of their structural and photophysical properties.

Experimental Section

Instrumentation methods used for characterization of the newly prepared platinum(II) complexes, photophysical and spectroscopic studies together with the characterization data for compounds **1**−**4** are described in the Supporting Information.

Synthesis of [Pt(bzq)Cl(CN-^{t}Bu)] (1). CN^{t}Bu (28 μL, 0.244 mmol) was added to a yellow suspension of [{Pt(bzq)(μ-Cl)}$_2$] (0.100 g, 0.122 mmol) in CH_2Cl_2 (15 mL) to give an orange solution. After stirring at room temperature for 5 min, the solvent was evaporated to 1 mL, and *n*-hexane (2 mL) was added. By cooling at −30 °C, **1** precipitated as an orange solid (0.084 g, 70%). In some cases, the product obtained was not pure, and it was recrystallized from $CHCl_3$/*n*-hexane at −30 °C.

Synthesis of [Pt(bzq)Cl(CN-Xyl)] (2). To a yellow suspension of [{Pt(bzq)(μ-Cl)}$_2$] (0.100 g, 0.122 mmol) in CH_2Cl_2 (15 mL), CN-Xyl (0.032 g, 0.244 mmol) was added, to immediately give an orange solution. After 1 h of stirring, the solvent was removed in vacuo to 2 mL causing the precipitation of **2** as a yellow solid (0.082 g, 62%).

Reaction of [Pt(bzq)(μ-Cl)]$_2$ and CN-2-Np. Synthesis of [Pt(bzq)Cl(CN-2-Np)] (3) and [Pt(bzq)Cl_2][Pt(bzq)(CN-2-Np)$_2$] (4). To a yellow suspension of [{Pt(bzq)(μ-Cl)}$_2$] (0.100 g, 0.122 mmol) in CH_2Cl_2 (15 mL), CN-2-Np (0.037 g, 0.244 mmol) was added, and a red solution was obtained. After 1 h of stirring, the solvent was evaporated to 2 mL, and the addition of 5 mL of acetone resulted in the precipitation of a garnet-red solid, identified as a mixture of **3** and **4** (∼ratio 1:1). The mixture was heated at 150 °C for 1 h, and **3** was obtained as a yellow solid (0.070 g, 51%).

Synthesis of [Pt(bzq)Cl_2][Pt(bzq)(CN-2-Np)$_2$] (4). [Pt(bzq)-(CN-2-Np)$_2$]PF_6 (0.049 g, 0.059 mmol) was added over a yellow suspension of NBu_4[Pt(bzq)Cl_2] (0.040 g, 0.059 mmol) in acetone (15 mL), and a red suspension was immediately obtained. After 1 min of stirring, the suspension was filtered, and **4** was obtained as a garnet-red solid (0.056 g, 84%).

Computational Details. The computational method used was DFT with the B3LYP exchange-correlation functional,[89−91] using the Gaussian 03[92] program package. The basis set used was the LanL2DZ effective core potential for the platinum atom, and 6-31G(d,p) for the remaining atoms. TD-DFT calculations were carried out combined with the conductor-like polarizable continuum model approach (CPCM) implemented in the Gaussian 03 software to study the nature of the singlet−singlet transitions in the absorption spectra of **1**−**3** (CH_2Cl_2 as solvent). The unrestricted (U)B3LYP was used to optimize the low-lying triplet states of all the complexes for the investigation of the nature of the emission states. The vertical emission transitions were calculated also with a TD-DFT/CPCM approach with the model optimized for the T_1 state and CH_2Cl_2 as solvent. All the geometry optimizations were carried out with no symmetry constraint.

X-ray Structure Analysis of [1·0.5H_2O]$_2$, [1·$CHCl_3$]$_\infty$, 2, and [3·CH_2Cl_2]$_2$. Table 4 reports details of the structural analyses for all complexes. Yellow ([**1**·0.5H_2O]$_2$, **2**, [**3**·CH_2Cl_2]$_2$) or red ([**1**·$CHCl_3$]$_\infty$) crystals were obtained by slow diffusion of *n*-hexane into a CH_2Cl_2 ([**1**·0.5H_2O]$_2$, **2**, [**3**·CH_2Cl_2]$_2$) or $CHCl_3$ ([**1**·$CHCl_3$]$_\infty$) solution of each compound at low temperature (−30 °C). For complex [**1**]$_2$, two molecules of H_2O, for complex [**1**]$_\infty$ one of $CHCl_3$ and for complex [**3**·CH_2Cl_2]$_2$ one molecule of CH_2Cl_2 were found in the asymmetric unit ([**1**]$_2$, 0.5 molecules of H_2O and [**3**·CH_2Cl_2]$_2$, 0.5 molecules of CH_2Cl_2 per each molecule of the compound). X-ray data were collected with a NONIUS-κCCD area-detector ([**1**·0.5H_2O]$_2$, [**1**·$CHCl_3$]$_\infty$, **2**) or a Bruker Smart CCD ([**3**·CH_2Cl_2]$_2$) diffractometer, using graphite-monochromated Mo−K_α radiation (λ = 0.71073 Å). Images were processed using the DENZO and SCALEPACK software[93] for [**1**·0.5H_2O]$_2$, [**1**·$CHCl_3$]$_\infty$, and **2** (carrying out the absorption correction at this point for complex **2**) or the SAINT package for [**3**·CH_2Cl_2]$_2$. The absorption correction was performed using MULTISCAN[94] ([**1**·0.5H_2O]$_2$), XABS2[95] ([**1**·$CHCl_3$]$_\infty$), or SADABS[96] ([**3**·CH_2Cl_2]$_2$). The structures were solved by Patterson and Fourier methods using the DIRDIF92 program[97] ([**1**·0.5H_2O]$_2$) or Direct Methods ([**1**·$CHCl_3$]$_\infty$, **2**,

(89) Becke, A. D. *Phys. Rev. A: At., Mol., Opt. Phys.* **1988**, *38*, 3098.
(90) Lee, C.; Yang, W.; Parr, R. G. *Phys. Rev. B: Condens. Matter Mater. Phys.* **1988**, *37*, 785.
(91) Becke, A. D. *J. Chem. Phys.* **1993**, *98*, 5648.
(92) Frisch, M. J.; et al, Gaussian, Inc.: Wallingford, CT, 2004 (see Supporting Information for complete citation).
(93) Otwinowski, Z.; Minor, W. In *Methods in Enzymology*; Carter, C. V., Jr., Sweet, R. M., Eds.; Academic Press: New York, 1997; Vol. *276A*, p 307.
(94) Blessing, R. H. *Acta Crystallogr.* **1995**, *A51*, 33.
(95) Parkin, I. P.; Slawin, A. M. Z.; Williams, D. J.; Woolins, J. D. *Inorg. Chim. Acta* **1990**, *172*, 159.
(96) Sheldrick, G. M. *SHELXL-97, a program for crystal structure determination*; University of Göttingen, Göttingen, Germany, 1997.
(97) Beursken, P. T.; Beursken, G.; Bosman, W. P.; de Gelder, R.; García-Granda, S.; Gould, R. O.; Smith, J. M. M.; Smykalla, C. *The DIRDIF92 program system*; University of Nijmegen: The Netherlands, 1992.

Table 4. Crystal Data and Structure Refinement Parameters for Complexes $[\mathbf{1}\cdot\mathbf{0.5H_2O}]_2$, $[\mathbf{1}\cdot\mathbf{CHCl_3}]_\infty$, **2**, and $[\mathbf{3}\cdot\mathbf{CH_2Cl_2}]_2$

	$[\mathbf{1}\cdot\mathbf{0.5H_2O}]_2$	$[\mathbf{1}\cdot\mathbf{CHCl_3}]_\infty$	**2**	$[\mathbf{3}\cdot\mathbf{CH_2Cl_2}]_2$
empirical formula	$C_{18}H_{17}ClN_2O_{0.5}Pt$	$C_{19}H_{18}Cl_4N_2Pt$	$C_{22}H_{17}ClN_2Pt$	$C_{49}H_{32}Cl_4N_4Pt_2$
formula weight	499.88	611.24	539.92	1208.77
temperature (K)	173(1)	173(1)	173(1)	100(2)
wavelength (Å)	0.71073	0.71073	0.71073	0.71073
crystal system	triclinic	orthorhombic	monoclinic	monoclinic
space group	$P\bar{1}$	*Im*2*a*	$P2_1/c$	$P2_1/c$
crystal dimensions (mm)	0.325 × 0.25 × 0.25	0.20 × 0.175 × 0.05	0.175 × 0.175 × 0.025	0.29 × 0.28 × 0.21
a (Å)	13.7227(4)	6.6792(4)	15.5637(59	14.447(3)
b (Å)	13.7343(3)	13.2361(6)	7.5684(3)	19.399(4)
c (Å)	18.1103(5)	22.9268(13)	17.1981(6)	15.120(3)
α (deg)	94.668(2)	90	90	90
β (deg)	92.7050(10)	90	115.541(2)	105.974(4)
γ (deg)	90.712(2)	90	90	90
V (Å^3)	3397.71(16)	2026.88(19)	1827.84(11)	4073.5(16)
D_{calc} (Mg/m^3)	1.954	2.003	1.962	1.971
Z value	8	4	4	4
μ(Mo Kα) (mm^{-1})	8.418	7.456	7.830	7.166
F(000)	1904	1168	1032	2312
θ range (deg)	1.13 to 27.48	3.55 to 27.48	2.96 to 27.49	1.75 to 25.02
no. of reflns measd	52887	2516	4188	19465
no. of obsd reflns	12789	2420	3304	4633
Goodness of fit on F^{2a}	1.096	1.080	1.043	1.019
final *R* indices [$I > 2\sigma(I)$][a]	R1 = 0.0503, wR2 = 0.1199	R1 = 0.0327, wR2 = 0.0779	R1 = 0.0326, wR2 = 0.0615	R1 = 0.0529, wR2 = 0.1398
R indices (all data)	R1 = 0.0647, wR2 = 0.1295	R1 = 0.0360, wR2 = 0.0807	R1 = 0.0525, wR2 = 0.0698	R1 = 0.0855, wR2 = 0.1613
absolute structure parameter		0.558(14)		

[a] $R1 = \sum(|F_o| - |F_c|)/\sum|F_o|$; $wR2 = [\sum w(F_o^2 - F_c^2)^2/\sum wF_o^2]^{1/2}$; Goodness of fit $= \{\sum[w(F_o^2 - F_c^2)^2]/(N_{obs} - N_{param})\}^{1/2}$; $w = [\sigma^2(F_o^2) + (g_1P)^2 + g_2P]^{-1}$; $P = [\max(F_o^2;0) + 2F_c^2]/3$.

$[\mathbf{3}\cdot\mathbf{CH_2Cl_2}]_2$) and refined by full-matrix least-squares on F^2 with SHELXL-97.[98] The hydrogen atoms were constrained to idealized geometries and assigned isotropic displacement parameters equal to 1.2 times the U_{iso} values of their respective attached carbon for the aromatic and CH_2 hydrogen atoms and that of 1.5 for the methyl groups. Complex $[\mathbf{1}\cdot\mathbf{CHCl_3}]_\infty$ crystallizes in the non-centrosymmetric, polar, and achiral space group *Im*2*a*. The absolute structure parameter (0.558(14); 0.442 inverse configuration) shows that the crystal chosen for this analysis is an inversion twin. Thermal parameters of C17 were fixed as the average between its own parameters and those of C16 ones. To establish the identities of the N and metalated C atoms of the 7,8-benzoquinolinate ligand, the structures of $[\mathbf{1}\cdot\mathbf{CHCl_3}]_\infty$ and **2** were refined in 3 different ways (with the identities of the C and N of the ligand in one position, with the element types reversed, and with 50/50 hybrid scattering factor at each of the atomics sites). Examination of the ΔMSDA values for bonds involving theses atoms[99,100] revealed the assignment with the N atom *trans* to the isocyanide ligands. Final difference electron density maps showed some peaks above 1 e Å^{-3} for $[\mathbf{1}\cdot\mathbf{0.5H_2O}]_2$, $[\mathbf{1}\cdot\mathbf{CHCl_3}]_\infty$, and $[\mathbf{3}\cdot\mathbf{CH_2Cl_2}]_2$, most of them in the close vicinity of the Pt atoms or the solvent, with no chemical meaning.

Acknowledgment. This work was supported by the Spanish MICINN (Projects CTQ2008-06669-C02-01,02/BQU and CTQ2008-03860/BQU and a grant for A. Díez).

Supporting Information Available: Control by ^{1}H NMR spectroscopy of **4** to **3** (Figure S1). Absorption data for **1**−**4** at 298 K in different solvents (Table S1). UV−vis absorption spectra of **3** in different solvents and in different concentrations (Figure S2a−d). Emission data for **1**−**3** in toluene, 2-MeTHF and CH_3CN (5×10^{-5} M solutions at 298 K) (Table S2). Absorption spectra calculated from the reflectance spectra for **2**−**4** (Figure S3). Time-resolved emission profiles for $[\mathbf{1}]_2$ in solid state at 77 K (Figure S4). Excitation and emission spectra in the solid state at 298 K and at 77 K of **2** (Figure S5) and of **4** (Figure S6). Time resolved emission profiles of **2** in CH_2Cl_2 5×10^{-5} M at 298 K (Figure S7). Excitation and emission spectra in CH_2Cl_2 10^{-3} M at 298 K of **2** (Figure S8) and of **3** (Figure S9). Plots of the measurement luminescence decay constants versus concentration of **2** and **3** (Figure S10). Emission spectra in CH_2Cl_2 5×10^{-5} M at 77 K of **1**−**3** (Figure S11) and of **2** at different wavelengths (Figure S12). Emission spectra in CH_2Cl_2 10^{-3} M at 77 K of **1**−**3** (Figure S13). Drawings and Tables of DFT optimized atomic coordinates for ground state (S_0) of the optimized structures of **1**−**3** (Figures S14−S16 and Tables S3, S5 and S7). DFT optimized atomic coordinates for T_1 state of **1**−**3** (Tables S4, S6, and S8). Table of geometrical parameters of the optimized structures of **1**−**3** (Table S9). Representative frontier orbitals for **1**−**3** (Figures S17−S19). Selected low-lying singlet excited states (S_n) computed by TD-DFT/CPCM (CH_2Cl_2) for **1**−**3** with the orbitals involved, vertical excitation energies and assignments (Table S10). Diagrams of the single-electron transitions according to TD-DFT calculations (CH_2Cl_2) for the lowest-energy emissions for **1**−**3** (Figures S20−S22). Instrumentation methods used for characterization of the newly prepared platinum(II) complexes, photophysical and spectroscopic studies, and characterization data of **1**−**4**. Crystallographic data in CIF format. This material is available free of charge via the Internet at http://pubs.acs.org.

(98) Sheldrick, G. M. *SHELX-97 a program for the refinement of crystal structures*; University of Göttingen: Göttingen, Germany, 1997.
(99) Speck, A. L. *Acta Crystallogr.* **1990**, *A46*, C.
(100) Hirshfeld, F. *Acta Crystallogr., Sect. A* **1976**, *32*, 239.